Computational and Structural Biotechnology Journal 21 (2023) 899–909

Contents lists available at ScienceDirect

Computational and Structural Biotechnology Journal

journal homepage: www.elsevier.com/locate/csbj

Identification of crucial amino acid residues involved in large ring cyclodextrin synthesis by amylomaltase from Corynebacterium glutamicum

Sirikul Ngawiset [a,1], Abbas Ismail [a,1], Shuichiro Murakami [b], Piamsook Pongsawasdi [c], Thanyada Rungrotmongkol [a,d], Kuakarun Krusong [a,*]

[a] Center of Excellence in Structural and Computational Biology, Department of Biochemistry, Faculty of Science, Chulalongkorn University, Bangkok 10330, Thailand
[b] Department of Agricultural Chemistry, School of Agriculture, Meiji University, Kawasaki-shi, Kanagawa 214–8571, Japan
[c] Starch and Cyclodextrin Research Unit, Department of Biochemistry, Faculty of Science, Chulalongkorn University, Bangkok 10330, Thailand
[d] Program in Bioinformatics and Computational Chemistry, Graduate School, Chulalongkorn University, Bangkok 10330, Thailand

ARTICLE INFO

Article history:
Received 18 October 2022
Received in revised form 8 January 2023
Accepted 9 January 2023
Available online 10 January 2023

Keywords:
Amylomaltase
Corynebacterium glutamicum
Large-ring cyclodextrin
Molecular dynamic simulation
Site-directed mutagenesis

ABSTRACT

Amylomaltase can be used to synthesize large ring cyclodextrins (LR-CDs), applied as drug solubilizer, gene delivery vehicle and protein aggregation suppressor. This study aims to determine the functional amino acid positions of *Corynebacterium glutamicum* amylomaltase (*Cg*AM) involved in LR-CD synthesis by site-directed mutagenesis approach and molecular dynamic simulation. Mutants named Δ167, Y23A, P228Y, E231Y, A413F and G417F were constructed, purified, and characterized. The truncated *Cg*AM, Δ167 exhibited no starch transglycosylation activity, indicating that the N-terminal domain of *Cg*AM is necessary for enzyme activity. The P228Y, A413F and G417F produced larger LR-CDs from CD36-CD40 as compared to CD29 by WT. A413F and G417F mutants produced significantly low LR-CD yield compared to the WT. The A413F mutation affected all tested enzyme activities (starch tranglycosylation, disproportionation and cyclization), while the G417F mutation hindered the cyclization activity. P228Y mutation significantly lowered the k_{cat} of disproportionation activity, while E231Y mutant exhibited much higher k_{cat} and K_m values for starch transglycosylation, compared to that of the WT. In addition, Y23A mutation affected the kinetic parameters of starch transglycosylation and cyclization. Molecular dynamic simulation further confirmed these mutations' impacts on the *Cg*AM and LR-CD interactions. Identified functional amino acids for LR-CD synthesis may serve as a model for future modification to improve the properties and yield of LR-CDs.

1. Introduction

Amylomaltase from mesophilic *Corynebacterium glutamicum* (*Cg*AM) bacterium belongs to glycoside hydrolase family 77 (GH77) and the enzyme catalyzed four enzymatic reactions including: (i) hydrolysis of an α-1,4-glycosidic linkage; (ii) disproportionation or a transfer of an α-1,4-glucan to another α-1,4-glucan acceptor; (iii) cyclization or intramolecular transglycosylation; and (iv) coupling or a reverse reaction of cyclization [1]. To date, AMs have demonstrated wide applications related to starch modification and processing leading to several functional products. The main interest of AM is the ability to synthesize highly sought cyclic glucans, or large ring cyclodextrins (LR-CDs), with a degree of polymerization (DP) of more than eight through intramolecular transglycosylation reaction [2–4].

The LR-CDs are highly soluble in water and relatively have a larger hydrophobic cavity compared to the small ring cyclodextrin. These distinct properties have been extensively manipulated for biotechnological applications. For example, LR-CDs are increasingly pursued as gene delivery vehicles and solubility enhancers through inclusion complexation for poorly water-soluble drugs [5–7], as

Abbreviations: *Cg*AM, *Corynebacterium glutamicum* amylomaltase; HPAEC-PAD, High Performance Anion Exchange Chromatography with Pulsed Amperometric Detection; LR-CDs, Large ring cyclodextrins; MD, molecular dynamic; RMSD, root mean square displacement; WT, wild type amylomaltase

* Corresponding author.
E-mail address: Kuakarun.k@chula.ac.th (K. Krusong).
[1] S. Ngawiset and A. Ismail are co-first authors.

https://doi.org/10.1016/j.csbj.2023.01.011

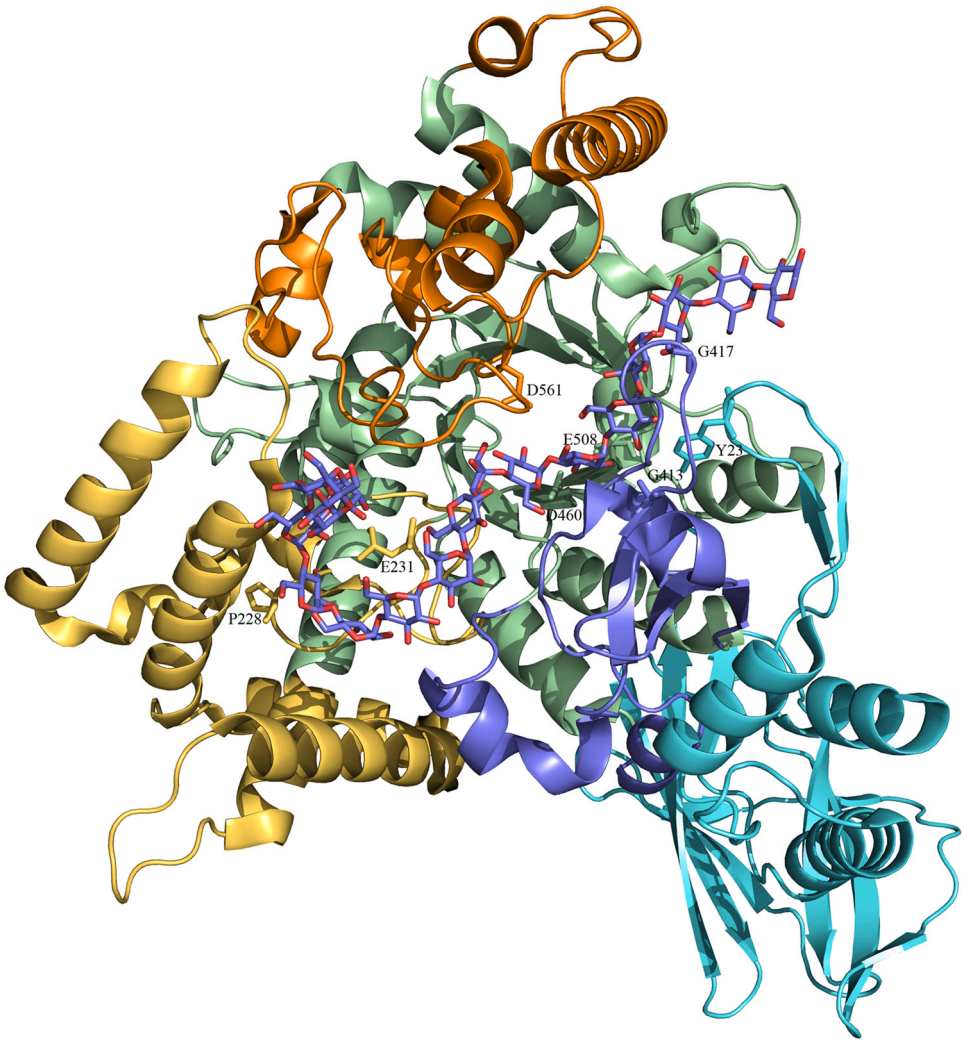

Fig. 1. Structure of *Cg*AM with cycloamylose residues 1–16 (superimposed of cocrystal *Ta*AM and cycloamylose structure (PDB entry 5jiw) on *Cg*AM structure (PDB entry 5b68)). The N-terminal domain, the $(\beta/\alpha)_8$ –barrel and the three auxiliary subdomains CA1, CA2 and CA3 of *Cg*AM are shown in cyan, green, yellow, blue and orange, respectively. The catalytic residues of *Cg*AM are D460, E508 and D561. The mutated amino acid residues in this study are Y23, P228, E231, A413 and G417.

opposed to traditional polymer materials [8]. Compared to the polymer, LR-CDs simplify the process without molecular modification and offer high biocompatibility and high biodegradability with lower toxicity. Moreover, the ability of LR-CDs to accommodate large molecules makes it a good stripping agent by effectively stripping the detergent in the protein refolding process and preventing aggregation during the process [9]. Protein folding persists as one of the major concerns in protein expression and the use of LR-CDs in protein refolding bears a significant development. Besides that, AM has shown potential application in food industry such as in the synthesis of functional linear oligosaccharides via intermolecular transglycosylation reaction on starch, which contributes to meet the "healthy" food demand [3,10]. With the ability to modify the starch structure, the AM also has been used in the production of commercially available thermoreversible starch gel and replacement for gelatin in food products [11–13].

At present, in addition to *Cg*AM [14], there are several other three-dimensional (3D) structures of GH77 AM from different bacteria that have been deposited including from *Thermus acuatiqus* (*Ta*AM) [15], *Thermus thermophilus* (*Tt*AM) [16], *Thermus brockianus* (*Tb*AM) [17] and *Streptococcus agalactiae* (*Sa*AM) [18]. The 3D structure of *Cg*AM (Fig. 1) was illustrated to composed of N- (Met1-Arg165) and C- (Leu166-Asp706) terminal domains, which can be further divided into N1 and N2 subdomains. Besides, the C-domain consists of one core subdomain and three auxiliary subdomains (CA1, CA2, CA3) [14]. The catalytic residues of *Cg*AM are D460, E508 and D561 which correspond to D293, E340 and D395 in *Ta*AM, respectively. CA subdomains are highly involved in the formation of substrate binding pocket where the CA2 is the major contributor. Overall, the *Cg*AM structure highly matched to other AMs with two apparent differences at the C- domain, where *Cg*AM has a unique structure at the connecting loop in the CA1 subdomain and extended α − helices in the CA3 subdomain. These structural differences could affect the substrate specificity and substrate binding mechanism of the *Cg*AM [14]. Additionally, *Cg*AM has the distinct functionally unknown N-domain that is also present in *Escherichia coli* AM (*Ec*AM), while non-existent in other AMs [11]. The in-silico analysis recently reported that the N-domain presumably functions in starch binding [19].

Previously, several mutations were found to alter *Cg*AM properties. The mutations normally changed the thermostability, catalytic efficiency, LR-CD product yield and LR-CD size selectivity [11]. For example, A406V *Cg*AM showed higher thermostability and gave higher amount of LR-CD products, in comparison to the WT enzyme [20]. Y172A mutations caused a shift of principal LR-CDs to the larger size products [21], while N287Y mutant exhibited higher thermostability, changed LR-CD profile and increased substrate preference for maltoheptaose (G5) [22]. Besides that, mutation Y418A/D/S at the

loop of *Cg*AM shifted the principal product to larger DPs of LR-CDs [23]. Yet, to date, how the mutations may affect the *Cg*AM structures and conformations that contribute to the altered performance and characteristics has not been wholly revealed in detail. This lack of information could hinder the development of enzyme modifications to improve and customize desired end products.

In this study, we aim to investigate multiple potential functional amino acids in *Cg*AM that are involved in LR-CD synthesis and examine the effect of the mutations on enzyme conformation and interactions. Herein, we focus on the role of the N-domain and the amino acid residues Y23, E231, P228, A413 and G417 of *Cg*AM (Fig. 1). The Y23 is a part of the channel for amylose binding found on the N-terminal domain of *Cg*AM, which is absent in *Ta*AM [14]. Meanwhile, the E231 and P228 at the CA1 that are equivalent to Y54 and Y101 in *Ta*AM, were proposed as the second binding site and played a role in hydrophobic interaction with the substrate to form LR-CDs [24]. G413 and G417 are located on the CA2 of *Cg*AM or equivalent to the 250 loop in *Ta*AM that facilitate the transglycosylation and cyclization reactions [11]. In addition, molecular dynamic simulations were performed to understand the interaction between the wild-type *Cg*AM and resulted mutants with CD25.

2. Materials and methods

2.1. Plasmid constructions and mutagenesis

The *Cg*AM gene (2121 bp) was inserted into two plasmid constructs named *Cg*AM-pET17b and *Cg*AM-pET19b [21,25]. The former expressed non-fusion *Cg*AM, while the latter produced a His-tagged fusion protein. QuickChange™ Site-directed mutagenesis was employed using a pair of complementary primers with a mutation (Supplementary data, Table S1) to generate Y23A, P228Y, E231Y, A413F and G417F mutants. *Cg*AM-pET17b was used as a template to create Y23A and E231Y mutations, while *Cg*AM-pET19b was used for making P228Y, A413F and G417F mutations. In addition, the truncated *Cg*AM gene encoding amino acid 168–706, Δ167, was subcloned through *Nde* I and *Not* I restriction sites into expression vector pMAL-c5X (New England BioLabs Inc.), creating Δ167 mutant. All mutants were verified by sequencing.

2.2. Protein expression and purification

Non-fusion and His-tagged WT *Cg*AM were expressed and purified as described previously [21,25]. All mutant enzymes were expressed in *E. coli* BL21(DE3). Mutants Y23A, P228Y and E231Y were grown in LB broth containing 100 μg/ml ampicillin, while A413F and G417F were cultured in the medium with 100 μg/ml ampicillin and 1 % glucose. The cultures were grown at 37 °C to A_{600} = 0.4–0.6 before induction with 1 mM isopropylthio-β-D-galactoside (IPTG) at 16 °C for 6 h (Y23A) or 18 h (P228Y, E231Y, A413F and G417F). The cultures were harvested and lysed by sonication. After removing cell debris by centrifugation, the non-fusion mutants (Y23A and E231Y) were purified by a two-column process (HiTrap DEAE FF and HiPrep Phenyl FF (High Sub) columns (GE Healthcare), while His-tagged fusion enzymes (P228Y, A413F and G417F) were purified by HisTrap FF column (GE Healthcare). These mutant enzymes were purified in the same manner of the WT *Cg*AM [21,25].

The truncated *Cg*AM, Δ167 was expressed in *E. coli* BL21 codon plus (DE3), cultured in LB broth containing 100 μg/ml ampicillin and 34 μg/ml chloramphenicol with the addition of 1 % glucose. The Δ167 gene with maltose binding protein (MBP) tag at the N-terminus was induced by 1 mM IPTG for 6 h at 16 °C and purified by Amylose Resin High Flow (New England BioLabs Inc.). In brief, Δ167 in 50 mM phosphate buffer, pH 7.4 was loaded onto an amylose column and unbound proteins were removed. Δ167 was then eluted from the column using a buffer containing 10 mM maltose. Factor Xa was used to cleave MBP-tag on Δ167 (1 mg Factor Xa for a reaction containing 100 mg fusion protein) for 16 h at 4 °C. The cleaved protein was reloaded onto an amylose column and the unbound protein was collected.

The purity of the protein was determined by sodium dodecyl sulfate polyacrylamide gel electrophoresis (SDS-PAGE) and the concentration of protein was measured by Pierce® BCA Protein Assay Kit (Thermo Scientific).

2.3. Enzyme assays

Starch transglycosylation, starch degradation, disproportionation, hydrolysis, cyclization and coupling activities of the WT and mutants were performed as described previously [21,26]. All assays were done in triplicate.

2.4. Effect of pH and temperature on enzyme activity and stability

Starch transglycosylation activity of the WT and mutants were assayed in buffer with pH range of 3.5–10.0, in order to determine the optimum pH of the enzyme. The optimum temperature was examined at the temperature range of 20–70 °C. In addition, pH and temperature stability were investigated by measuring remaining activity after the enzyme was pre-incubated at pH 3.5–10.0 or temperature of 20–70 °C for 1 h.

2.5. Substrate specificity

Disproportionation activity was used to determine substrate specificity of the WT and mutants. Enzyme of 0.05 U disproportionation activity was incubated with 50 mM malto-oligosaccharides (maltose (G2) to maltoheptaose (G7)) in phosphate buffer pH 6.0 at 30 °C for 10 min. The reaction was stopped by addition of 1 N HCl and the amount of glucose was detected by glucose oxidase method [27].

2.6. Synthesis and analysis of LR-CDs

Enzyme of 0.05 U starch degradation activity was incubated with 0.2% (w/v) pea starch in 50 mM phosphate buffer pH 6.0 at 30 °C for 6, 12 and 24 h. The reaction was stopped by boiling for 10 min. Then, the mixture was incubated with 8 U of glucoamylase from *Rhizopus* sp. (Sorachim, France) at 40 °C for 16 h and heat-inactivated for 10 min. The reaction product was analyzed by high-performance anion-exchange chromatography-pulsed amperometric detection (HPAEC-PAD) using Carbopac PA-100 column (4 × 250 mm, Dionex, USA) as described elsewhere [21,28]. The size of the LR-CD products was compared with the sizes of the standard LR-CDs that had been determined by matrix-assisted laser desorption/ionization-time of flight MALDI-TOF [29] mass spectrometry.

2.7. Analysis of kinetic parameters

Kinetic parameters of three reactions, including starch transglycosylation, disproportionation, and cyclization of the WT and mutants were investigated. The Michaelis-Menten kinetic parameters, K_m and V_{max} were determined from the Lineweaver - Burk plot and used to calculate the turnover number, k_{cat} and the specificity constant, k_{cat}/K_m. To determine kinetic parameters, WT and mutant enzymes were incubated with varied concentrations of substrate in 50 mM phosphate buffer (pH 6.0 for WT and pH 6.5 for mutants). For starch transglycosylation, the enzyme was incubated with 0.05 % soluble starch and various concentration of glucose (0 – 10 mM) at 30 °C for 20 min; and the rate of reaction was measured by iodine method [30]. For disproportionation, enzyme was incubated with different amounts of maltotriose (0–200 mM) at 30 °C for 10 min;

and the rate of reaction was calculated from the amount of glucose in the reaction, assayed by glucose oxidase method [27]. Cyclization reaction was set up by incubating the enzyme with pea starch (0 – 5 mg/mL), dissolved in 3 % DMSO at 30 °C for 1 h. After stopping the reaction by boiling and treated with 8 U of glucoamylase, the amount of LR-CDs was measured by HPAEC-PAD.

2.8. Circular dichroism (CD) spectroscopy

Secondary structures of WT and mutants *Cg*AM were determined using Spectropolarimeter (J-815CD spectrometer, JASCO, Japan). Spectra of protein samples (0.2 mg/mL) were recorded between 190 and 240 nm at 25 °C. K2D3 server program was used to predict protein secondary structure (http://cbdm-01.zdv.uni-mainz.de/~andrade/k2d3//index.html) [31].

2.8.1. Computational analysis

3D structure of *Cg*AM (PDB: 5B68) [14] was downloaded and deleted all miscellaneous atoms in PDB file by Accelrys Discovery Studio 2.5 (Accelrys Software Inc.). Oligosaccharide (G11) was built and minimized. To predict the molecular interactions between target protein and ligand, *Cg*AM and oligosaccharide were docked via SwissDock web server. An α-1,4 D glucan was added to the ligand molecule until the size of CD increased up to 25 molecules in cyclic conformation. The starting models for molecular dynamics (MD) simulation were prepared and minimized by AMBER14 package program [32]. Interaction analysis of *Cg*AM-CD25 complex was performed by MD simulations under a periodic boundary condition with the isothermal-isobaric ensemble where the number of moles (N), pressure (P) and temperature (T) were kept constant. All covalent bonds involving hydrogen atoms in each system was constrained with the SHAKE algorithm [33]. The short-range cutoff of 10 Å for nonbonded interactions was applied, while the particle mesh Ewald (PME) summation method [34] was used for calculating the long-range electrostatic interactions. The simulation time step was 0.2 ps. The system was initially heated up to 298 K for 200 ps and then simulated at this temperature at 1 atm till 50 ns. The trajectories were collected in every 2 ps and analyzed as follows:

2.9. The stability of global structure

To determine the stability of the complex system in MD simulation, root mean square deviation (RMSD) was reported using the PTRAJ module of AMBER. RMSD of all atoms relative to those of initial structure versus the simulation time was plotted.

2.10. Flexibility of protein structure

To determine the flexibility of the complex system in MD simulation, RMSF and B-factor were reported. RMSF graph was plotted in the time range of 30 – 50 ns and B-factor was visualized by VMD program.

2.11. Hydrogen bond interactions

H-bond was explored using PTRAJ module of AMBER. The criteria of H-bond are as follows: (i) the distance between H-bond donor and acceptor atoms is less than or equal to 3.5 Angstrom (ii) the angle of H-bond must be more than 120 degree.

2.12. Binding free energy and key residues of ligand binding

The binding free energy (ΔG_{bind}) was calculated by molecular mechanics with generalized Born and surface area solvation (MM/GBSA) approach using mm_pbsa module [35–37]. In this study, MM/GBSA was applied to estimate the $\Delta\Delta G_{bind}$ between *Cg*AM and ligand (CD25) by computing $\Delta\Delta G_{bind}$ as the free energy difference between the complex (ΔG_{cpx}), protein (ΔG_{prot}), and ligand (ΔG_{lig}) as follows: $\Delta G_{bind} = \Delta G_{cpx} - (\Delta G_{prot} + \Delta G_{lig})$. Each term was obtained from the averaged free energy over 100 trajectories taken from the last 20-ns simulation. The key residue was determined and analyzed from per-residue decomposition free energy calculation.

Model of *Cg*AM mutants in complex with CD25 was generated and analyzed using the same procedure to study the WT *Cg*AM-CD25 complex.

3. Results and discussions

3.1. Enzyme expression, purification and characterization

This work aims to identify the important amino acids for *Cg*AM activity. Site-directed mutagenesis, enzyme characterization and MD simulations were employed. From amino acids sequence analysis, *Cg*AM exhibited 27.7 % identity and 43.7 % similarity to *Ec*AM [38], while showing low sequence identity to *Ta*AM (16.2 % identity and 23.8 % similarity) [39], 16.3% identity to *Tt*AM (16.4 % identity and 23.8 % similarity) [39], *Tf*AM (17.7 % identity and 26.6 % similarity) [29], *Thermotoga maritima* (11.9 % identity and 20.3 % similarity) [40], *Aquifex aeolicus* (15.8 % identity and 25.2 % similarity) [41] and *Streptococcus pneumoniae* (16.2 % identity and 27.5 % similarity) [42] as calculated by EMBOSS Needle program [43]. Since both *C. glutamicum* and *E. coli* are mesophilic bacteria, *Cg*AM is more similar to *Ec*AM than AMs from other microorganisms and possibly share similar mechanism.

In this research, the WT crude extract from *E. coli* BL21 (DE3) transformed by *Cg*AM-pET17b and *Cg*AM-pET19b contained 2.0 and 2.3 U/mg of specific activity for transglycosylation reaction, as shown in Table S2 which is similar to previous reports [21,25]. The specificity activities of WT enzymes produced in pET17b and pET19b expression vectors were not different. However, the transglycosylation specific activity of P228Y, E231Y, A413F and G417F crude *Cg*AM were 2.7, 2.2, 2.0 and 1.9 U/mg, respectively. Furthermore, the WT and mutated *Cg*AM (Δ167, Y23A, E231Y, P228Y, A413F and G417F) were successfully expressed and purified (Supplementary data, Fig. S1-S3 and Table S2). In brief, non-fusion and His-tagged wild-type *Cg*AM showed similar specific activity on starch transglycosylation at 42.8 and 48.2 U/mg, respectively indicating that His-tagged has no influence on *Cg*AMs activity (Table S2). The truncated *Cg*AM, Δ167, showed no starch transglycosylation activity, indicating that the N-terminal domain of *Cg*AM is required for starch transglycosylation activity. Among all mutants, excluding Δ167, the A413F *Cg*AM possessed the lowest specific activity, in comparison to the WT. It is worth mentioning that the Y23A *Cg*AM showed higher specific activity, compared with the WT.

3.2. Enzyme activity and kinetic

The activities of AM were observed via 6 reactions: starch transglycosylation, starch degradation, disproportionation, cyclization, coupling and hydrolysis activity. WT, P228Y, E231Y and G417F had similar specific activities of starch transglycosylation and starch degradation (Table 1), suggesting that P228Y, E231Y and G417F mutations had no strong effects on starch transglycosylation and starch degradation. However, P228Y mutation seemed to affect disproportionation activity. This indicated that P228 may be important for catalysis of short-chain oligosaccharides but not long-chain carbohydrate such as starch. It is also worth noting that the mutations showed little effect on cyclization reaction for all mutants except A413F. The WT exhibited cyclization specific activity at 0.0012 U/mg, while P228Y, E231Y and G417F mutants showed the same level of specific activity at range 0.0007–0.0013 U/mg.

Table 1
Specific activity of wild type and mutated *Cg*AM.

*Cg*AM activity	Specific activity (U/mg protein)					
	WT	Y23A	P228Y	E231Y	A413F	G417F
Starch transglycosylation[a]	59.9 ± 2.29	58.6 ± 1.37	52.2 ± 0.54	61.2 ± 1.10	18.8 ± 1.99	52.3 ± 1.07
Disproportionation[b]	43.5 ± 0.64	40.5 ± 1.08	16.3 ± 1.05	50.2 ± 1.36	9.04 ± 1.05	53.5 ± 1.21
Starch degradation[c]	0.37 ± 0.02	0.37 ± 0.01	0.32 ± 0.01	0.37 ± 0.00	0.11 ± 0.02	0.31 ± 0.01
Cyclization[d]	0.0012 ± 0.0005	0.0008 ± 0.0002	0.0009 ± 0.0001	0.0013 ± 0.0001	0.0001 ± 0.0001	0.0007 ± 0.0003
Coupling[e]	0.0012 ± 0.0007	0.0004 ± 0.0000	0.0002 ± 0.0001	0.0010 ± 0.0005	0.0001 ± 0.0001	0.0004 ± 0.0001
Hydrolysis[f]	0.03 ± 0.00	0.02 ± 0.00	0.02 ± 0.00	0.02 ± 0.00	0.01 ± 0.00	0.03 ± 0.00

*Data are mean ± S.D. from three independent repeats
(a) Starch transglycosylation activity was assayed using 0.2 % (w/v) soluble potato starch and 1 % (w/v) maltose as substrates. One unit was defined as the amount of enzyme that produced 1 % decrease in color of the starch-iodine complex.
(b) Disproportionation was assayed using 5 % maltotriose as a substrate and the reaction was measured by glucose oxidase method. One unit was defined as the amount of enzyme which produced 1 μmol of glucose per min.
(c) Starch degradation was measured using 0.75 % (w/v) soluble starch and iodine method. One unit was defined as the amount of enzyme that degraded 1 mg per mL of starch per min.
(d) Cyclization reaction was performed using 2 % (w/w) pea starch as a substrate and LR-CD products were measured by HPAEC-PAD. One unit of enzyme was defined as the amount of enzyme which produced 1 nC of total LR-CDs per min.
(e) Coupling reaction was set using 3 mg/mL of LR-CDs and 1 mg/mL of cellobiose as substrates. The amount of released sugar was measured by DNS assay. One unit was the amount of enzyme that produced 1 μmol of reduced glucose per min.
(f) Hydrolysis of LR-CDs (0.5 mg/mL) was measured by bicinchoninic acid (BCA) method. One unit was defined as the amount of enzyme required to produce 1 μmol of reducing sugar per min.

Interestingly, the A413F exhibited significantly lower activity in all reactions, including starch transglycosylation, starch degradation, disproportionation and cyclization than the WT enzyme by 3.19, 4.81 and 3.36 times, respectively. A413F and G417F located on the CA2 subdomain which is equivalent to the location of 400 s and 250 s loops found in *Ec*AM [44] and *Ta*AM, respectively [45]. These conformational flexible long extended loops (400 s and 250 s) are highly homologous among the amylomaltases and suggested to be involved in substrate binding at the reducing end of scissile bond and regulating the enzyme activity [15, 17, 44]. Both of mutants were mutated from the aliphatic side chain to the aromatic side chain which reduced the flexibility of the loop. Therefore, this study strongly suggested that at least for *Cg*AM, the A413 plays a key role in substrate binding and regulating the starch transglycosylation, starch degradation, disproportionation and cyclization reactions.

In general, AM enzymes showed lower coupling activity, in comparison to that of CGTase enzyme [46]. From Table 1, WT and E231Y had similar coupling activity, while Y23A, P228Y, A413F and G417F showed less coupling activity than the WT enzyme.

Due to low specific activity of A413F in all measured reactions (Table 1), only four mutants (Y23A, P228Y, E231Y and G417F) were further analyzed in kinetic study. The kinetic parameters of starch transglycosylation, disproportionation and cyclization are shown in Table 2. P228Y, E231Y and G417F had similar k_{cat}/K_m values for starch transglycosylation to that of the WT *Cg*AM (k_{cat}/K_m = 5.74 ± 0.78 mM^{-1} min^{-1}), while Y23A exhibited significantly lower k_{cat}/K_m (k_{cat}/K_m = 2.69 ± 0.19 mM^{-1} min^{-1}), in comparison to that of the WT. Y23A mutation caused higher K_m, indicating that this mutation affected the binding of starch.

When compared disproportionation kinetic of the WT to that of the mutants, Y23A and E231Y showed k_{cat}/K_m of $5.43 \times 10^2 \pm 0.95$ and $4.24 \times 10^2 \pm 0.36$ mM^{-1} min^{-1}, respectively, which were higher than that of the WT enzyme (k_{cat}/K_m = $3.42 \times 10^2 \pm 0.53$ mM^{-1} min^{-1}). These two mutants possessed lower K_m, so it is possible that Y23 and E231 are involved in the binding of malto-oligosaccharides. In addition, P228Y mutant was observed with significantly lower catalytic efficiency of the disproportionation reaction, compared with that of the WT. Reduction of k_{cat}/K_m value of P228Y for disproportionation activity was due to low k_{cat} value, suggesting that P228Y mutation hampered turnover rate of the enzyme. The low disproportion activity of P228Y implied that P228Y may prefer substrate longer than G3 such as starch, which in contrast to E231Y and the WT. Moreover, the effect of low disproportionation activity could be due to the increase in hydrophobic interaction in the CA1 with the introduction of tyrosine. This result is supported by the previous mutation study that reported N287Y mutant in the CA1 subdomain also exhibited a low value of k_{cat}/K_m compared to the WT [22].

Table 2
Kinetic parameters of wild type and mutants *Cg*AM.

	Starch Transglycosylation		
	K_m (mM) $[10^{-2}]$	k_{cat} $(min^{-1})[10^{-1}]$	k_{cat}/K_m $(mM^{-1}\ min^{-1})$
WT	8.22 ± 2.63	4.37 ± 0.60	5.74 ± 0.78
Y23A	14.0 ± 2.28	3.75 ± 0.50	2.69 ± 0.19
P228Y	7.41 ± 0.00	4.37 ± 0.60	5.92 ± 0.98
E231Y	18.6 ± 2.33	10.76 ± 0.68	5.74 ± 0.64
G417F	7.18 ± 1.31	3.27 ± 0.38	4.64 ± 0.76
	Disproportionation Activity		
	K_m (mM)	**k_{cat} $(min^{-1})[10^3]$**	**k_{cat}/K_m $(mM^{-1}\ min^{-1})$ $[10^2]$**
WT	18.1 ± 2.28	6.18 ± 1.11	3.42 ± 0.53
Y23A	12.27 ± 0.34	6.65 ± 1.06	5.43 ± 0.95
P228Y	19.7 ± 4.74	2.63 ± 0.22	1.39 ± 0.34
E231Y	15.4 ± 6.03	6.68 ± 3.65	4.24 ± 0.36
G417F	22.9 ± 3.04	8.37 ± 0.03	3.69 ± 0.48
	Cyclization Activity		
	K_m (mg/ml)	**k_{cat} $(min^{-1})[10^{-2}]$**	**k_{cat}/K_m (ml/mg/min) $[10^{-2}]$**
WT	6.14 ± 0.55	16.64 ± 4.24	2.73 ± 0.75
Y23A	2.75 ± 0.62	9.43 ± 1.16	3.48 ± 0.38
P228Y	5.71 ± 1.45	13.68 ± 2.55	2.41 ± 0.22
E231Y	5.33 ± 0.52	16.75 ± 3.62	2.97 ± 1.26
G417F	2.38 ± 0.26	4.53 ± 0.45	1.92 ± 0.22

*Data are mean ± S.D. and derived from Lineweaver-Burk plots from three independent repeats

For cyclization reaction, the Y23A exhibited slightly higher k_{cat}/K_m for cyclization activity compared to the WT (WT, k_{cat}/K_m = $2.73 \times 10^{-2} \pm 0.75$ ml/mg/min; Y23A, k_{cat}/K_m = $3.48 \times 10^{-2} \pm 0.38$ mL/mg/min). Although Y23A showed a lower k_{cat} value compared to the WT, it had a significantly lower K_m value. This indicated that at a slower reaction rate relative to the WT, the catalytic efficiency was compensated by a much higher affinity of the substrate toward Y23A compared to the WT. Both P288Y and E231Y demonstrated the same level of k_{cat}/K_m value for cyclization reaction compared to the WT, which indicated that the mutation at P228 and E231 did not impact the inter and intra transglycosylation capability of the enzyme when using starch as the substrate. Meanwhile, the G417F mutant gave significantly lower k_{cat} and K_m values in cyclization reaction when compared to that of WT, which implied that the mutation affected both substrate catalysis and binding.

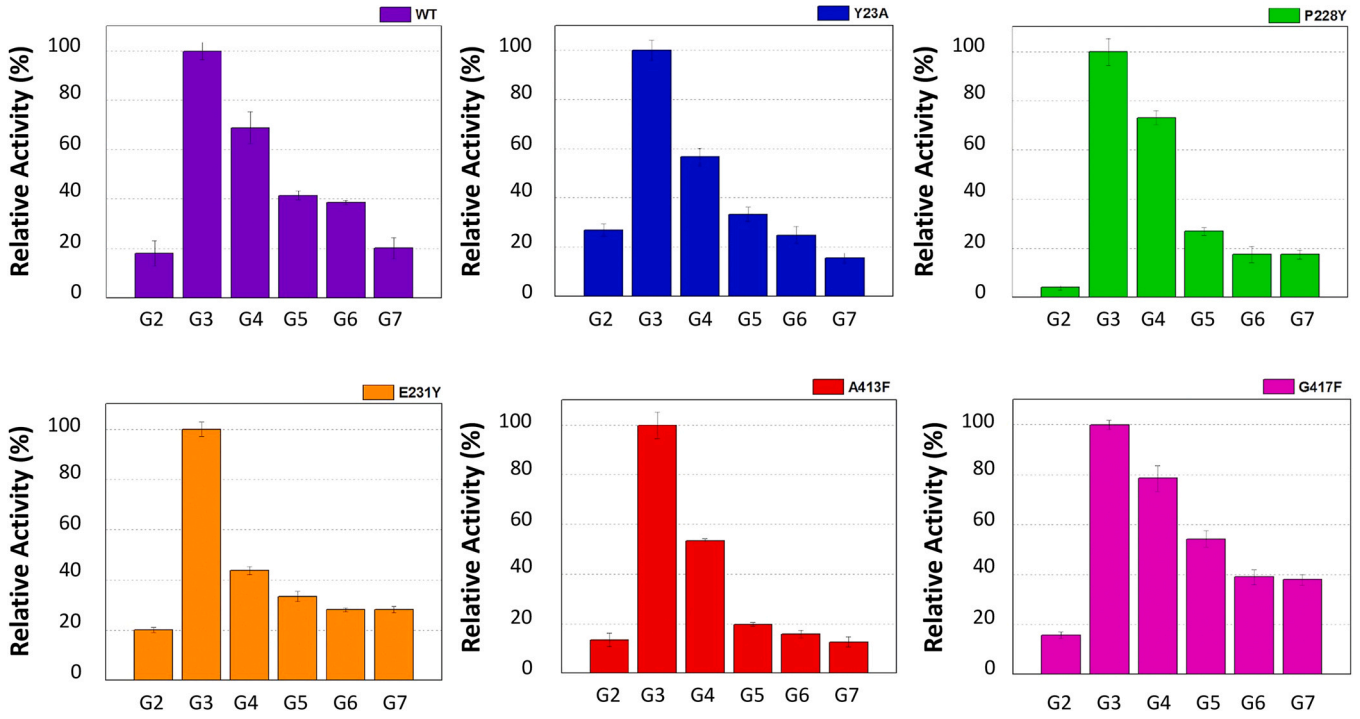

Fig. 2. Substrate specificity of wild-type and mutated *Cg*AMs in disproportionation reaction using malto-oligosaccharides (G2-G7) as substrate. The activity of *Cg*AM on G3 substrate was 100%. Data are presented as the mean SD derived from triplicate experiments.

3.3. Substrate specificity

Substrate specificity of AM in disproportionation reaction was investigated by various oligosaccharides (G2 – G7) as a substrate (Fig. 2). The WT and all mutants were observed to prefer maltotriose (G3) over other substrates. The descending order of preferred substrate was G3 > G4 > G5~ G6-G7 > G2. Similarly, the previous research on *Cg*AM also showed that G3 is the preferred substrate for the WT and its mutants named Y172A, A406V, A406L and N287Y [20–22, 47]. Moreover, AM from other organisms such as *Thermus thermophilus* HB8 [16] and *Pyrobaculum aerophilum* IM2 [48] also had the same order of substrate preference. However, the pattern of substrate specificity of *Tf*AM was different (G3 > G4~ G5 > G7 > G6 > > G2) [29]. Our findings showed that the point mutations on *Cg*AM at the selected amino acids did not affect the substrate specificity of the enzyme.

3.4. Optimum and stability of temperature and pH

WT and mutants showed similar optimum temperature and temperature stability (Supplementary data, Fig. S4 and S5). The WT *Cg*AM showed the optimum temperature at 30 °C and temperature stability in a range of 20–35 °C, while all mutants had similar optimum temperature (25–35 °C) and temperature stability (20–40 °C). When the temperature increased up to 40 °C, all enzymes lost their activity. Generally, all enzymes were stable and maintained their activity at 20 °C for 1 h. When the temperature increased from 30 °C to 70 °C, the activity of all mutants decreased and finally lost all activity. It is worth noting that only E231Y demonstrated more stability than the WT at 30–35 °C. At 35 °C incubation, the remaining activity of WT was approximately 60 % while E231Y retained activity above 80%. This finding indicated that the mutation at E231 has improved the thermostability of the enzyme which is also exhibited by *Cg*AM mutant A406V from the previous study [20].

Meanwhile, all mutants in this study, excluding A413F, showed no significant changes in optimum pH and pH stability, compared with the WT (Supplementary data, Fig. S6 and S7). WT and all mutants except A413F possessed optimum pH at 6–6.5 and pH stability in a broad range of pH 5.0–10.0. Meanwhile, A413F mutant showed optimum pH at 7.5 and retained its activity above 80% in a narrow pH range (pH 5.0–6.5).

The optimum pH range of *Cg*AM in our study is in accordance with the previous report of *Cg*AM [20–22, 25], while other AM enzymes from *Thermus sp.*, for example, the *Ta*AM prefer a slightly acidic medium at pH 5.5 [49]. Meanwhile, the optimum temperature for starch transglycosylation of *Cg*AM was similar to other mesophilic bacteria such as *E. coli* (35 °C) [50], *Synechocystis* sp. (45 °C) [51], *Pseudomonas stutzari* (37 °C) [52]. In contrast, AM from thermophilic bacteria *Thermus sp.* like *Ta*AM (75 °C) [39,49] and *Tf*AM (60 °C) [29] normally demonstrated high activity at extremely high temperatures.

3.5. LR-CD synthesis

Fig. 3 showed LR-CD production profiles of WT and mutated *Cg*AM. At 6 h incubation, the major LR-CDs produced by WT, Y23A, E231Y and A413F were CD29, CD25, CD27 and CD40, respectively. Meanwhile, G417F and P228Y produced mostly CD36. For comparison, *Tf*AM produced CD25 – CD29 as a principal product at 4 h incubation [29]. Prolong incubation at 12 h has shifted the principal LR-CDs that were produced by WT, E231Y, A413F and G417F where the dominant LR-CDs changed to smaller sizes as CD27, CD25, CD38 and CD32, respectively. Meanwhile, the sizes of LR-CDs by Y23A and P228Y were unaffected. At 24 h incubation, the LR-CDs size further decreased for WT and A413F to CD24 and CD33, respectively, whereas LR-CDs by Y23A showed a slight increase in size from CD25 to CD26. Meanwhile P228Y, E231Y and G417F maintained a similar size of LR-CDs as 12 h incubation.

The LR-CD size distribution was decreased at long hour incubation as exhibited by WT and all mutants except the Y23A and P228Y. This result in accordance to previous studies on *Cg*AM enzyme [20–22, 25] and others AMs such as *Ta*AM [39], *Tf*AM [29] and potato

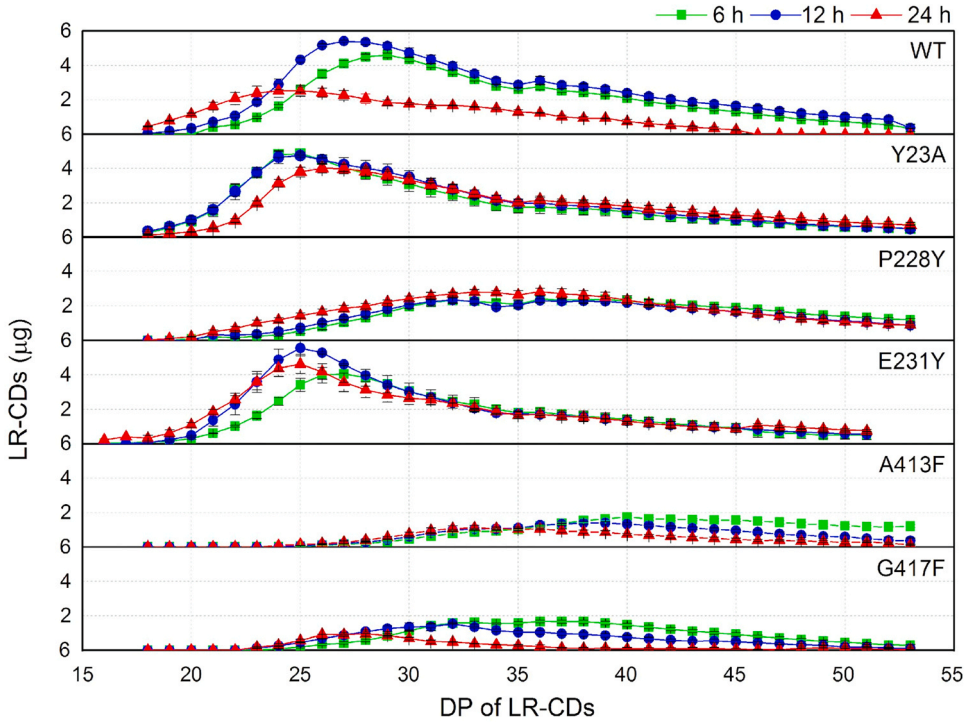

Fig. 3. LR-CD production profile of wild-type and mutated *Cg*AMs. Enzyme (0.05 U) was incubated with 0.2% (w/v) pea starch for 6, 12 and 24 h, then LR-CDs were analyzed by HPAEC-PAD. Data are shown as the mean SD derived from three independent experiments.

D enzyme [53]. Principal LR-CDs from all mutants were different from WT where the E231Y and Y23A gave smaller LR-CDs while other mutants (P228Y, A413F and G417F) gave larger products. This showed that changing the side chain amino acid to more hydrophobic side chain (P to Y and A/G to F), calculated from pH 7 system [54] at the positions 228, 413 and 417 of *Cg*AM has increased the size of LR-CD products. It is previously shown that hydrophobic interactions are important for globular confirmation, and it is likely that changes of amino acids in these positions have altered the conformation stability leading to interfering with substrate binding as discussed earlier [20]. Additionally, P228 is located at the secondary binding site, which is important for the formation of LR-CDs due to hydrophobic interaction with the substrate. Therefore, adding more hydrophobicity to the CA1 (E231/P228) and CA2 (A413/G417) sites affected cyclization activity which resulted in the formation of different LR-CD sizes compared to the WT.

The percentage yield of LR-CD production from all mutants was observed to be lower than the WT. In contrast, A406V, A406L and N287Y of *Cg*AM mutants from the previous study gave higher yields than the WT [20]. Meanwhile, the amount of LR-CD products from P228Y at 6 h, 12 h and 24 h incubation time did not significantly change which could be due to the coupling reaction of the enzyme as previously mentioned. However, it is worth noting that A413F and G417F mutants produced significantly less amount of LR-CDs than the WT, but with larger major product sizes as shown in Fig. 3. This finding supports the notion mentioned earlier based on enzyme activities that the mutations at A413 and G417 on the CA2 subdomain to Phe that contained aromatic ring side chain, have decreased the flexibility of the loop leading to jeopardized substrate binding and affecting the product size of LR-CDs. The A413 and G417 are in the loop region that is equivalent to the 250 s loop found in *Ta*AM and *Tb*AM where the flexibility of the loop was previously reported to be important in substrate binding and formation of cyclic products [17,45]. Additionally, decreases in the mutants' flexibility were also demonstrated in the MD simulation results as described in Section 3.7.2.

3.6. Secondary structure

Circular dichroism spectra showed that the WT and mutants exhibited similar overall secondary structure content (Supplementary data**,** Fig. S8). This implies that these point mutations do not disturb the overall structure.

3.7. Computational analysis

After the starting models for MD simulation were prepared and minimized, analysis results from MD were reported as follows:

3.7.1. Stability of global structure

To determine the stability of all complex systems in MD simulation, RMSDs of all atoms relative to those of initial structure versus the simulation time were plotted (Supplementary data, Fig. S9). The RMSD values of complex atoms increased in the first 10 ns and fluctuated around 2–3 Å till 50 ns. All complexes tend to be stabilized after 20 ns. In all cases, ligands showed higher RMSD values in comparison with those of *Cg*AM-CD25 complexes. At 30 – 50 ns, the ligands in the WT-CD25 and P228Y-CD25 models displayed higher RMSD values than those in other mutant-CD25 complexes, indicating that the ligands in these two complexes were more flexible. Next, the MD trajectories from 30 to 50 ns of these systems were extracted for further analysis.

3.7.2. Flexibility of protein structure

To evaluate flexibility of structure dynamics and fluctuation of each amino acids of *Cg*AM during MD simulation, RMSF and B-factor were investigated over the last 20 ns of the MD trajectories. The pattern of RMSF values suggested that the amino acids in the position of 150–250 and 400–500 (the CA2 subdomain and a part of core structure $(\alpha/\beta)_8$ barrel) were less fluctuated than amino acid residues in other regions (Supplementary data**,** Fig. S10). B-factor analysis illustrates rigid (dark blue) and flexible areas (light color) in protein structures. The active site of *Cg*AM was shown in a dark blue,

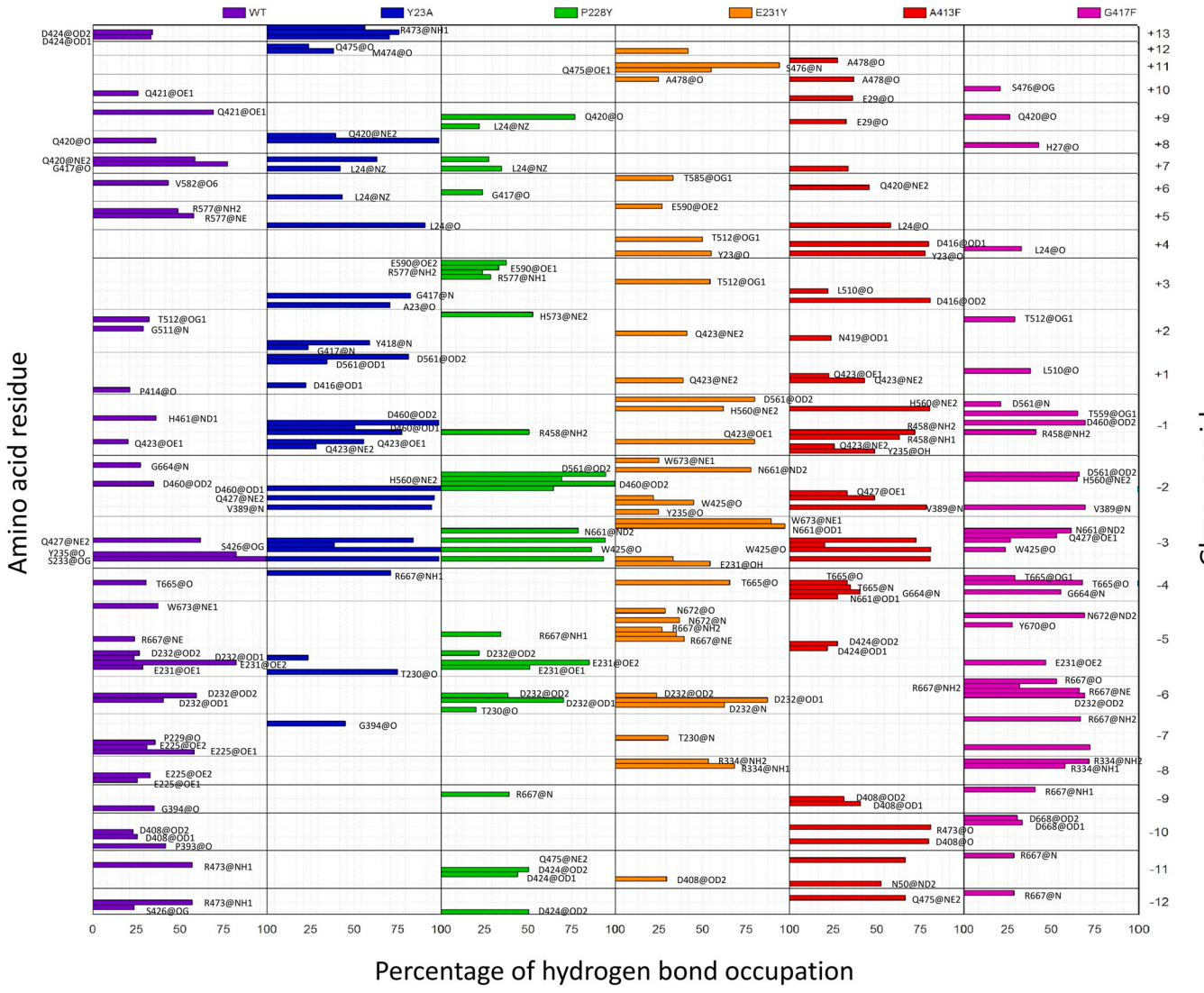

Fig. 4. Hydrogen bond occupation between CD25 (glucose residues at subsite −12 to +13) and amino acid residues in *Cg*AM. Each color showed WT *Cg*AM (purple) and the mutants, Y23A (blue), P228 (green), E231Y (orange), A413F (red) and G417F (pink). The order of the bar graph depends on the position of amino acid residues, interacting with glucose moieties in *Cg*AM-CD25 complexes. Cleavage takes place between the − 1 and + 1 subsites, where *-n* represents the non-reducing end and *+n* is the reducing end [55].

indicating a rigid structure, while the surface area of *Cg*AM was more flexible as displayed in a lighter color (Supplementary data, Fig. S11).

3.7.3. Hydrogen bond interactions

The intramolecular hydrogen bonding interactions (H-bond) between *Cg*AM and ligand (CD25) are essential for the strength of the complex. The hydrogen bond occupations between *Cg*AM and CD25 are shown in Fig. 4. The result demonstrated that the maximum % hydrogen bond occupation for the wild-type *Cg*AM-CD25 complex was 99.33 %, which was the H-bond between S233 and the glucose residue in subsite − 3. The catalytic residue D460 also showed H-bond interaction with CD25 at subsite − 2. E231 in the WT-CD25 complex formed H-bond with glucose residue in subsite − 5 with 82.19 % and 28.62 % of hydrogen bond occupation with the two carboxylate oxygens OE2 and OE1 of E231, respectively. In addition, the carbonyl group of G417 in the WT-CD25 complex formed H-bond with glucose residue in subsite + 7. Y23, P228 and A413 showed no % hydrogen bond occupation with glucose residues, however, the adjacent residues P229 and P414 displayed % hydrogen bond occupation of 35.76 % and 21.33 % with glucose in subsites − 7 and + 1, respectively.

Similar to the WT-CD25 complex, the Y23A, P228Y, E231Y, A413F mutants-CD25 complexes showed the H-bond between S233 and the glucose residue in subsite − 3, but this H-bond formation was absent in G417F-CD25 complex. Y23A mutation caused the adjacent residue L24 to form H-bond with glucose residues in subsites + 6 and + 7 and the catalytic residues D561 and D460 formed H-bond with glucose residues in subsites + 1 and − 1, respectively. In the P228Y-CD25 complex, the catalytic residues D561 and D460 displayed H-bond interactions with the glucose in subsite − 2. E231Y mutation enhanced H-bond interactions between D232 and glucose residues in subsite − 6, compared with the WT enzyme; and the catalytic residue D561 of E231Y mutant formed H-bond with CD25 at subsite − 1. No H-bond interactions between the catalytic residues D561 and D460 were observed in the A413F-CD25 complexes. This may explain why A413F showed low cyclization activity. Furthermore, based on *Cg*AM structure analysis, mutation of alanine at position 413 to phenylalanine may result in a crash of F413 with Y23 (Supplementary data, Fig. S12), and this may cause a significant decrease of enzyme activity. Meanwhile, G417F showed H-bond interactions between D561 and D460 and glucose residue in subsites − 2 and − 1, respectively.

Table 3
Energy components and average binding free energies (kcal/mol) for CgAM-CD25 complexes calculated by MM/GBSA approach.

	WT-CD25	Y23A-CD25	P228Y-CD25	E231Y-CD25	A413F-CD25	G417F-CD25
ΔE_{ELE}	-250.5 ± 30.9	-218.2 ± 16.9	-219.0 ± 33.3	-230.7 ± 35.3	-278.1 ± 25.8	-309.4 ± 25.2
ΔE_{VDW}	-192.1 ± 10.0	-181.5 ± 9.0	-171.8 ± 9.1	-194.6 ± 9.9	-189.9 ± 8.7	-198.2 ± 10.4
ΔE_{MM}	-442.6 ± 35.7	-399.8 ± 19.4	-390.8 ± 36.0	-425.3 ± 35.9	-468.0 ± 24.9	-507.6 ± 27.2
$\Delta G_{NONPOLAR,SOL}$	-26.0 ± 1.6	-25.2 ± 1.0	-23.5 ± 1.2	-27.3 ± 1.2	-27.5 ± 0.9	-27.8 ± 0.9
$\Delta G_{ELE,SOL}$	381.3 ± 31.5	333.6 ± 14.9	329.8 ± 28.7	370.4 ± 32.8	405.2 ± 19.2	422.1 ± 22.7
ΔG_{SOL}	355.3 ± 30.4	308.4 ± 14.6	306.3 ± 28.0	343.1 ± 32.2	377.7 ± 18.8	394.3 ± 22.2
$T\Delta S$	-49.1 ± 13.9	-52.5 ± 18.7	-53.8 ± 14.6	-46.8 ± 15.30	- 45.6 ± 16.3	-47.8 ± 14.1
ΔG_{TOTAL}	-38.2	-38.8	-30.7	-35.4	-44.6	-65.5

3.7.4. Key residues of ligand binding

Table 3 showed the energy components and average binding free energies for *Cg*AM-CD25 complexes calculated by MM/GBSA approach. The binding free energy (ΔG_{total}) for WT and mutated *Cg*AM-CD25 were −38.2 kcal/mol (wild-type), −38.8 kcal/mol (Y23A), −30.7 kcal/mol (P228Y), −35.4 kcal/mol (E231Y), −44.6 kcal/mol (A413F) and −65.5 kcal/mol (G417F). As shown in Table 3, ΔE_{vdW} and ΔE_{ele} contributed to the binding of *Cg*AM with CD25, while the polar solvent energy (ΔG_{sol}) impeded the binding. In all cases, ΔG_{total} values were negative, indicating a favor complex formation.

Fig. 5 showed per-residue decomposition free energy for WT and mutants in complex with CD25. The results demonstrated key residues in the binding of *Cg*AM to CD25. The positive and negative values of per-residue decomposition energy specify the ligand destabilized and stabilized, respectively. The key binding residues that had the per-residue decomposition free energy less than −1 kcal/mol were reported. As shown in Fig. 5, it is likely that amino acid residues in the C-terminal domain (residue 390–680) play a major part in CD25 binding. Clearly, a different set of amino acid residues in the WT and mutants contributes to complex formation. In the WT-CD25 complex, W425 showed the lowest energy (−6.10 kcal/mol). It implies that W425 is the key residue for stabilizing the WT-CD25 complex. In addition, Y23, E231 and G417 displayed negative values of per-residue decomposition energy and assisted in stabilization of the complex. Other amino acid residues, including L236, G394, Q420, F534, R577 and W673, involved in the WT-CD25 complex. For catalytic residues (D460, E508 and D561), the total energy of each residue in the complex was high (ΔE = +), especially D460. Y23A mutation resulted in more negative value of per-residue decomposition energy at position 23, in comparison to that of the WT. This indicated that the substitution of tyrosine to alanine at position 23 enhanced CD25 binding at this position. In contrast, E231Y and G417F yielded higher energy, compared to the WT, suggesting that these mutations lowered CD25 binding ability at positions 231 and 417 respectively.

As shown in Table 3, the average binding free energies for Y23A-CD25 and E231Y-CD25 complexes were similar to the WT-CD25 complex and this may contribute to similar yield and size distribution of LR-CDs in Fig. 3. In contrast, A413F-CD25 and G417F-CD25 complexes possessed higher average binding free energies (ΔGtotal =

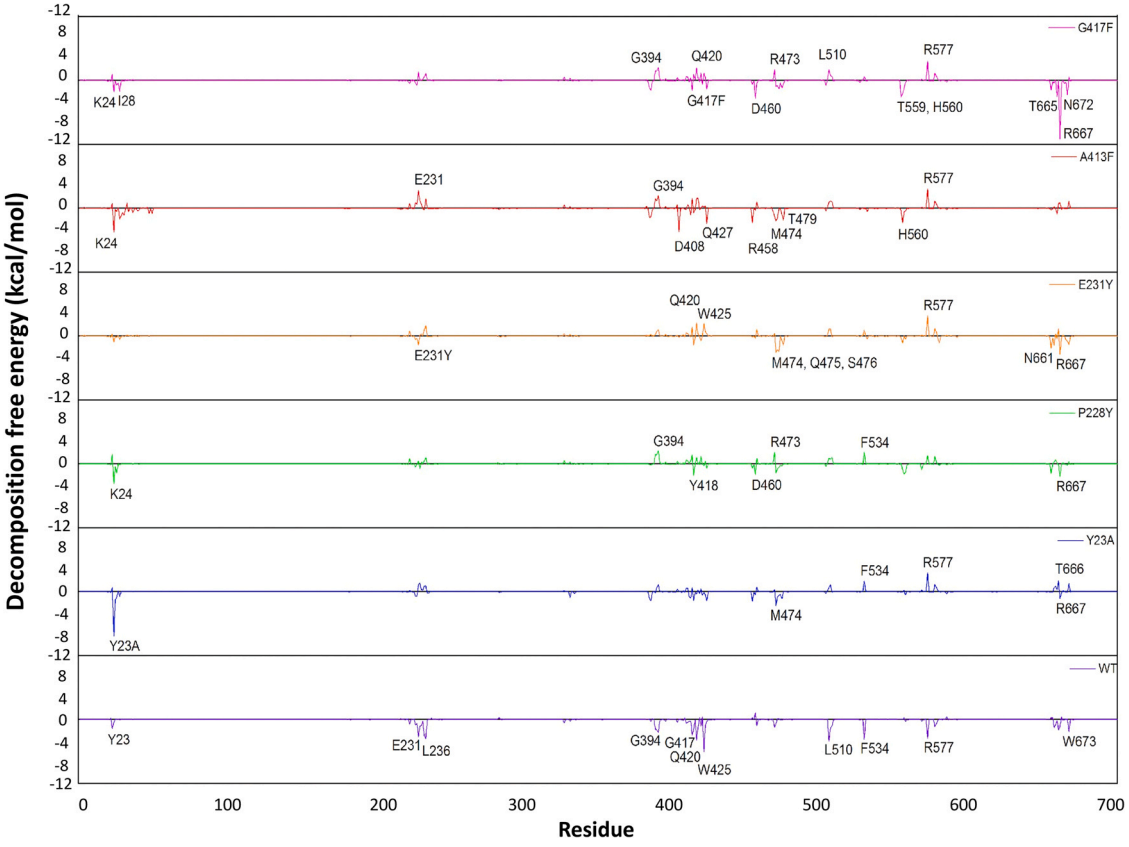

Fig. 5. Per-residue decomposition free energy obtained from MM/GBSA calculation for WT and mutant *Cg*AMs in complex with CD25. Each color represented WT *Cg*AM (purple) and the mutants, Y23A (blue), P228 (green), E231Y (orange), A413F (red) and G417F (pink).

−44.6 kcal/mol for A413F-CD25 and −65.5 kcal/mol for G417F-CD25, in Table 3) than that of the WT-CD25 complex (−38.2 kcal/mol). This tight complex formation may hinder cyclization reaction, resulting in lower yield of LR-CDs by A413F and G417F mutants, compared with the WT. Regarding ΔE_{ELE}, G417F mutation significantly altered electrostatic interactions in the *Cg*AM-CD25 complex.

Meanwhile, P228Y-CD25 complex showed a lower ΔG_{total} (Table 3), compared to that of the WT enzyme. In addition, P228Y mutation caused a shift of principal LR-CDs to larger- size products (Fig. 3), which is in contrast with E231Y mutation, showing a slight shift of principal LR-CDs towards smaller-size products. Both P228Y and E231Y possessed similar kinetic parameters for cyclization to that of the WT enzyme (Table 2).

Based on the kinetics parameters, Y23A mutation seemed to affect starch transglycosylation, but not disproportionation (Table 2). Although Y23A mutant showed lower k_{cat} and K_m for cyclization, compared with the WT enzyme, the k_{cat}/K_m of Y23A and ΔG_{total} for Y23A-CD25 were similar to that of the WT.

4. Conclusion

The present study provides insight into the importance of mutated amino acids in *Cg*AM for LR-CD synthesis. The N-domain was found to be important in starch transglycosylation reaction, in which the deletion of the domain significantly hampered the transglycosylation reaction. Mutations at several points in the subdomain CA1 and CA2 affected the *Cg*AM starch modification reactions, leading to different size profiles of LR-CDs compared to the WT. A413F and G417F mutants significantly reduced the LR-CD yield, indicating the importance of flexibility in the loop region of *Cg*AM in substrate binding and cyclization reaction. Identified key amino acids in *Cg*AM and their effects on the product synthesis may serve as a model for future application in the production of more highly functional biomaterials.

CRediT authorship contribution statement

Sirikul Ngawiset: Investigation, Formal analysis, Validation, Visualization. **Abbas Ismail:** Validation, Visualization, Writing – original draft. **Shuichiro Murakami:** Resources, Supervision. **Piamsook Pongsawasdi:** Resources, Supervision. **Thanyada Rungrotmongkol:** Resources, Supervision, Methodology, Validation, Visualization, Writing – review & editing. **Kuakarun Krusong:** Conceptualization, Investigation, Methodology, Resources, Validation, Visualization, Writing – original draft, Supervision, Project administration, Funding acquisition.

Declaration of Competing Interest

The authors declare that they have no known competing financial interests or personal relationships that could have appeared to influence the work reported in this paper.

Acknowledgements

We thank Mr.Thanarat Pathomsoonthornchai for conducting preliminary experiments on E231Y. SN was supported by Chulalongkorn University Graduate Scholarship to commemorate the 72nd Anniversary of His Majesty King Bhumibol Adulyadej and received the Overseas Research Experience Scholarship for Graduate Student from the Graduate School and Department of Biochemistry, the Faculty of Science, Chulalongkorn University, Thailand, for a short-term research visit at Graduate School of Agriculture, Meiji University, Japan. This research was funded by The Asahi Glass Foundation and partial support came from the 90th Year Chulalongkorn Scholarship. TR and KK have been supported by Center of Excellence in Structural and Computational Biology and the C2F Postdoctoral Fellowship to AI. SM, PP and KK acknowledged travel supports from Core-to-Core Program (JSPS-NRCT).

Appendix A. Supporting information

Supplementary data associated with this article can be found in the online version at doi:10.1016/j.csbj.2023.01.011.

References

[1] Lombard V, Golaconda Ramulu H, Drula E, Coutinho PM, Henrissat B. The carbohydrate-active enzymes database (CAZy) in 2013. Nucleic Acids Res 2014;42:D490–5.
[2] Kuttiyawong K, Saehu S, Ito K, Pongsawasdi P. Synthesis of large-ring cyclodextrin from tapioca starch by amylomaltase and complex formation with Vitamin E acetate for solubility enhancement. Process Biochem 2015;50:2168–76.
[3] Kaulpiboon J, Poomipark N, Watanasatitarpa S. Expression and characterization of amylomaltase gene involved in the large-ring cyclodextrin and isomalto-oligosaccharide production. Sci & Technol Asia 2016:18–28.
[4] Suksiri P, Ismail A, Sirirattanachatchawan C, Wangpaiboon K, Muangsin N, Tananuwong K, Krusong K. Enhancement of large ring cyclodextrin production using pretreated starch by glycogen debranching enzyme from *Corynebacterium glutamicum*. Int J Biol Macromol 2021;193:81–7.
[5] Ismail A, Kerdpol K, Rungrotmongkol T, Tananuwong K, Ueno T, Ekasit S, Muangsin N, Krusong K. Solubility enhancement of poorly water soluble domperidone by complexation with the large ring cyclodextrin. Int J Pharm 2021;606:120909.
[6] Kerdpol K, Nutho B, Krusong K, Poo-arporn RP, Rungrotmongkol T, Hannongbua S. Encapsulation of α-tocopherol in large-ring cyclodextrin containing 26 α-D-glucopyranose units: a molecular dynamics study. J Mol Liq 2021;339:116802.
[7] Tahara Y, Yasuoka J, Sawada S, Sasaki Y, Akiyoshi K. Effective CpG DNA delivery using amphiphilic cycloamylose nanogels. Biomater Sci 2015;3:256–64.
[8] Barclay TG, Day CM, Petrovsky N, Garg S. Review of polysaccharide particle-based functional drug delivery. Carbohydr Polym 2019;221:94–112.
[9] Machida S, Ogawa S, Xiaohua S, Takaha T, Fujii K, Hayashi K. Cycloamylose as an efficient artificial chaperone for protein refolding. FEBS Lett 2000;486:131–5.
[10] Saehu S, Srisimarat W, Prousoontorn MH, Pongsawasdi P. Transglucosylation reaction of amylomaltase for the synthesis of anticariogenic oligosaccharides. J Mol Catal B Enzym 2013;88:77–83.
[11] Krusong K, Ismail A, Wangpaiboon K, Pongsawasdi P. Production of large-ring cyclodextrins by amylomaltases. Molecules 2022;27.
[12] van der Maarel MJEC, Capron I, Euverink G-JW, Bos HT, Kaper T, Binnema DJ, Steeneken PAM. A novel thermoreversible gelling product made by enzymatic modification of starch. Starch/Stärke 2005;57:465–72.
[13] G.J.W. Euverink, D.J. Binnema, Use of modified starch as an agent for forming a thermoreversible gel, Google Patents, 2005.
[14] Joo S, Kim S, Seo H, Kim KJ. Crystal structure of amylomaltase from *Corynebacterium glutamicum*. J Agric Food Chem 2016;64:5662–70.
[15] Przylas I, Tomoo K, Terada Y, Takaha T, Fujii K, Saenger W, Sträter N. Crystal structure of amylomaltase from *Thermus Aquaticus*, a glycosyltransferase catalysing the production of large cyclic glucans. J Mol Biol 2000;296:873–86.
[16] Kaper T, Leemhuis H, Uitdehaag J, van der Veen B, Dijkstra B, van der Maarel M, Dijkhuizen L. Identification of acceptor substrate binding subsites +2 and +3 in the amylomaltase from *Thermus thermophilus*. Biochem 2007;46(5261–5269):HB8.
[17] Jung J, Jung T, Seo D, Yoon S, Choi C, Park B, Park C, Woo E. Structural and functional analysis of substrate recognition by the 250s loop in amylomaltase from *Thermus brockianus*. Proteins 2011;79:633–44.
[18] Tumhom S, Nimpiboon P, Wangkanont K, Pongsawasdi P. *Streptococcus agalactiae* amylomaltase offers insight into the transglycosylation mechanism and the molecular basis of thermostability among amylomaltases. Sci Rep 2021;11:6740.
[19] Marecek F, Moller MS, Svensson B, Janecek S. A putative novel starch-binding domain revealed by in silico analysis of the N-terminal domain in bacterial amylomaltases from the family. 3 Biotech 2021;11(229):GH77.
[20] Nimpiboon P, Kaulpiboon J, Krusong K, Nakamura S, Kidokoro S, Pongsawasdi P. Mutagenesis for improvement of activity and thermostability of amylomaltase from *Corynebacterium glutamicum*. Int J Biol Macromol 2016;86:820–8.
[21] Srisimarat W, Kaulpiboon J, Krusong K, Zimmermann W, Pongsawasdi P. Altered large-ring cyclodextrin product profile due to a mutation at Tyr-172 in the amylomaltase of *Corynebacterium glutamicum*. Appl Environ Microbiol 2012;78:7223–8.
[22] Nimpiboon P, Krusong K, Kaulpiboon J, Kidokoro S, Pongsawasdi P. Roles of N287 in catalysis and product formation of amylomaltase from *Corynebacterium glutamicum*. Biochem Biophys Res Commun 2016;478:759–64.
[23] Tumhom S, Krusong K, Pongsawasdi P. Y418 in 410s loop is required for high transglucosylation activity and large-ring cyclodextrin production of amylomaltase from *Corynebacterium glutamicum*. Biochem Biophys Res Commun 2017;488:516–21.

[24] Strater N, Przylas I, Saenger W, Terada Y, Fuji K, Takaha T. Structural basis of the synthesis of large cycloamyloses by amylomaltase. Biologia 2002;57:93–100.
[25] Srisimarat W, Powviriyakul A, Kaulpiboon J, Krusong K, Zimmermann W, Pongsawasdi P. A novel amylomaltase from *Corynebacterium glutamicum* and analysis of the large-ring cyclodextrin products. J Incl Phenom Macrocycl Chem 2011;70:369–75.
[26] Rachadech W, Nimpiboon P, Naumthong W, Nakapong S, Krusong K, Pongsawasdi P. Identification of essential tryptophan in amylomaltase from *Corynebacterium glutamic*um. Int J Biol Macromol 2015;76:230–5.
[27] Miwa OJ, Maeda I, Okuda G K. Mutarotase effect on colorimetric determination of blood glucose with β-D-glucose oxidase. Clin Chim Acta. 1972;37:538–40.
[28] Koizumi K, Sanbe H, Kubota Y, Terada Y, Takaha T. Isolation and characterization of cyclic alpha-(1→4)-glucans having degrees of polymerization 9-31 and their quantitative analysis by high-performance anion-exchange chromatography with pulsed amperometric detection. J Chromatogr A 1999;852:407–16.
[29] Kaewpathomsri P, Takahashi Y, Nakamura S, Kaulpiboon J, Kidokoro S-i, Murakami S, Krusong K, Pongsawasdi P. Characterization of amylomaltase from *Thermus filiformis* and the increase in alkaline and thermo-stability by E27R substitution. Process Biochem 2015;50:1814–24.
[30] Park J, Kim H, Kim Y, Cha H, Kim Y, Kim T, Kim Y, Park K. The action mode of *Thermus aquaticus* YT-1 4-α-glucanotransferase and its chimeric enzymes introduced with starch-binding domain on amylose and amylopectin. Carbohydr Polym 2007;67:164–73.
[31] Louis-Jeune C, Andrade-Navarro MA, Perez-Iratxeta C. Prediction of protein secondary structure from circular dichroism using theoretically derived spectra. Proteins 2012;80:374–81.
[32] Case DA, Babin V, Berryman JT, Betz RM, Cai Q, Cerutti DS, Cheatham III TE, Darden TA, Duke RE, Gohlke H, Goetz AW, Gusarov S, Homeyer N, Janowski P, Kaus J, Kolossváry I, Kovalenko A, Lee TS, LeGrand S, Luchko T, Luo R, Madej B, Merz KM, Paesani F, Roe DR, Roitberg A, Sagui C, Salomon-Ferrer R, Seabra G, Simmerling CL, Smith W, Swails J, Walker RC, Wang J, Wolf RM, Wu X, Kollman PA. AMBER14. San Francisco: University of California; 2014.
[33] Ryckaert J, Ciccotti G, Berendsen H. Numerical integration of the cartesian equations of motion of a system with constraints: molecular dynamics of *n*-alkanes. J. Comput. Phys. 1977;23:327–41.
[34] York D, Darden T, Pedersen L.) The effect of long-range electrostatic interations in simulations of macromolecular crystals: a comparison of the Ewald and truncated list methods. J Chem Phys 1993;99:8345–8.
[35] Hou T, Wang J, Li Y, Wang W. Assessing the performance of the MM/PBSA and MM/GBSA methods. 1. The accuracy of binding free energy calculations based on molecular dynamics simulations. J Chem Inf Model 2011;51:69–82.
[36] Li X, Zhang W, Qiao X, Xu X. Prediction of binding for a kind of non-peptic HCV NS3 serine protease inhibitors from plants by molecular docking and MM-PBSA method. Bioorg Med Chem 2007;15:220–6.
[37] Meeprasert A, Hannongbua S, Rungrotmongkol T. Key binding and susceptibility of NS3/4A serine protease inhibitors against hepatitis C virus. J Chem Inf Model 2014;54:1208–17.
[38] Krempl P, Mairhofer J, Striedner G, Thallinger G. Finished genome sequence of the laboratory strain *Escherichia coli* K-12 RV308 (ATCC 31608). Genome Announc 2014;2:e00971–009714.
[39] Terada Y, Fujii K, Takaha T, Okada S. *Thermus aquaticus* ATCC 33923 amylomaltase gene cloning and expression and enzyme characterization: production of cycloamylose. Appl Environ Microbiol 1999;65:910–5.
[40] Nelson KE, Clayton RA, Gill SR, Gwinn ML, Dodson RJ, Haft DH, Hickey EK, Peterson JD, Nelson WC, Ketchum KA, McDonald L, Utterback TR, Malek JA, Linher KD, Garrett MM, Stewart AM, Cotton MD, Pratt MS, Phillips CA, Richardson D, Heidelberg J, Sutton GG, Fleischmann RD, Eisen JA, White O, Salzberg SL, Smith HO, Venter JC, Fraser CM. Evidence for lateral gene transfer between archaea and bacteria from genome sequence of *Thermotoga maritima*. Nature 1999;399:323–9.
[41] Deckert G, Warren PV, Gaasterland T, Young WG, Lenox AL, Graham DE, Overbeek R, Snead MA, Keller M, Aujay M, Huber R, Feldman RA, Short JM, Olsen GJ, Swanson RV. The complete genome of the hyperthermophilic bacterium *Aquifex aeolicus*. Nature 1998;392:353–8.
[42] Lacks S, Dunn J, Greenberg B. Identification of base mismatches recognized by the heteroduplex-DNA-repair system of *Streptococcus pneumoniae*. Cell 1982;31:327–36.
[43] Rice P, Longden I, Bleasby A. EMBOSS: The european molecular biology open software suite. Trends Genet 2000;6:276–7.
[44] Weiss S, Skerra A, Schiefner A. Structural basis for the interconversion of maltodextrins by MalQ, the amylomaltase of *Escherichia coli*. J Biol Chem 2015;290:21352–64.
[45] Przylas I, Terada Y, Fujii K, Takaha T, Saenger W, Sträter N. X-ray structure of acarbose bound to amylomaltase from *Thermus aquaticus* implications for the synthesis of large cyclic glucans. Eur J Biochem 2000;267:6903–13.
[46] van der Veen B, Uitdehaag J, Dijkstra B, Dijkhuizen L. Engineering reaction and product specificity of cyclodextrin glycosyltransferase from *Bacillus circulans* strain 251. Biochim Biophys Acta Proteins Proteom 2000;1543:336–60.
[47] Srisimarat W, Murakami S, Pongsawasdi P, Krusong K. Crystallization and preliminary X-ray crystallographic analysis of the amylomaltase from *Corynebacterium glutamicum*. Acta Crystallogr F Struct Biol Commun 2013;69:1004–6.
[48] Kaper T, Talik B, Ettema T, Bos H, van der Maarel M, Dijkhuizen L. Amylomaltase of *Pyrobaculum aerophilum* IM2 produces thermoreversible starch gels. Appl Environ Microbiol 2005;71:5098–106.
[49] Fujii K, Minagawa H, Terada Y, Takaha T, Kuriki T, Shimada J, Kaneko H. Use of random and saturation mutagenesis to improve the properties of *Thermus aquaticus* amylomaltase for efficient production of cycloamyloses. Appl Environ Microbiol 2005;71:5823–7.
[50] Kitahata S, Murakami H, Okada S. Purification and some properties of amylomaltase from *Escherichia coli* IFO 3806. Agric Biol Chem 1989;53:2653–9.
[51] Lee B, Oh D, Yoo S. Characterization of 4-α-glucanotransferase from *Synechocystis* sp. PCC 6803 and its application to various corn starches. N Biotechnol 2009;26:29–36.
[52] Schmidt J, John M. Starch metabolism in *Pseudomonas stutzeri*. II. Purification and properties of a dextrin glycosyltransferase (D-enzyme) and amylomaltase Biochim. Biochim Biophys Acta 1979;566:100–14.
[53] Takaha T, Yanase M, Takata H, Okada S, Smith S. Potato D-enzyme catalyzes the cyclization of amylose to produce cycloamylose, a novel cyclic glucan. J Biol Chem 1996;271:2902–8.
[54] Monera O, Sereda T, Zhou N, Kay C, Hodges R. Relationship of sidechain hydrophobicity and alpha-helical propensity on the stability of the single-stranded amphipathic α-helix. J Pept Sci 1995;1:319–29.
[55] Davies GJ, Wilson KS, Henrissat B. Nomenclature for sugar-binding subsites in glycosyl hydrolases. Biochem J 1997;321:557–9.